The Table Mountain 8-mm-Wavelength Interferometer

M. A. Janssen, S. Gulkis, and E. T. Olsen
Planetary Atmosphere Section

B. L. Gary, F. S. Soltis, and N. I. Yamane
Microwave Observational Systems Section

A two-element radio interferometer operating at 8.33-mm wavelength has been developed at the Jet Propulsion Laboratory's Table Mountain Observatory near Wrightwood, CA. The interferometer employs a 5.5-m and a 3-m-diameter antenna on an east-west baseline of 60 or 120 m, yielding fringe spacings at transit of 28″ or 14″, respectively. The broad intermediate-frequency bandpass of 100-350 MHz and the system noise temperature of 500 K provide high sensitivity for the measurement of continuum sources. The interferometer has been used for high-resolution studies of the planets and the Sun, and it is currently being adapted to study solar flare emissions at high spatial and time resolution.

I. Introduction

We describe a millimeter-wavelength interferometer which has been developed at the Jet Propulsion Laboratory's Table Mountain Observatory, located in the San Gabriel Mountain range near Wrightwood, CA. The interferometer was designed for the observation of continuum sources at the fixed frequency of 36 GHz (8.33-mm wavelength), with the primary goal of performing high-resolution studies of solar system objects. For example the two available baselines permit disk-resolved observation of Venus, Jupiter, and Saturn. The receivers employ the lowest noise uncooled mixers currently available and a broad intermediate-frequency bandwidth to achieve maximum sensitivity.

The interferometer became operational in May 1974, and has been used for the measurement of the 8-mm brightness temperature of Saturn's rings (Ref. 1), limb darkening studies of the atmospheric emission from Venus and Jupiter, and a high-resolution study of the chromospheric emission from the quiet Sun (Ref. 2). Current and future observational projects include an investigation of the thermophysical properties of Mercury's surface and a program to obtain data on millimetric solar flare emissions.

II. Description

A. General

The principal elements of the interferometer are a 5.5-m and a 3-m-diameter antenna. The 3-m antenna is movable to one of two fixed stations located 60 and 120 m to the west of the larger antenna. These stations provide east-west baselines of 7,000 and 14,000 wavelengths and yield resolutions (fringe spacings) of 28″ and 14″, respectively, at source transit. To date the 3-m antenna has only been used at the 60-m station.

The altitude is 2290 m above mean sea level, placing the interferometer above the major portion of the atmosphere's water vapor.

A schematic of the interferometer is given in Fig. 1. One linear polarization of the source continuum is received in the neighborhood of the 36-GHz local oscillator (LO) frequency. This is downconverted by double-sideband superheterodyne receivers into the intermediate-frequency (IF) passband of 100-350 MHz. After amplification the IF signals are brought together through underground cabling and correlated to produce the output signal. This signal depends upon the spatial brightness structure of the source and its geometric relationship to the baseline (cf. Ref. 3).

Coherence at the correlator inputs requires (1) coherence of the LO signals in each receiver and (2) equal delay in each signal path between the source and the correlator. Coherent LO signals at 36 GHz are passively generated in each receiver from a single 12-GHz signal provided by a centrally located oscillator. This scheme eliminates the need for independent local oscillators and active phase-lock loops. The relative signal delay depends upon the source-baseline geometry, which varies with the earth's rotation, and is equalized by a computer-controlled delay compensation network.

The correlator performs an analog multiplication of the instantaneous voltages appearing at its two input ports. Provided the two local oscillators are perfectly coherent, a source in the antenna beams produces a sinusoidal signal with a frequency varying from zero to approximately 1 Hz. This frequency is due to the motion of the source through the interferometer fringe pattern, which is determined by the source-baseline geometry. To simplify data processing, a constant correlator output signal frequency of 0.5 Hz is maintained by introducing a small frequency offset into one local oscillator signal.

B. Antennas

The 5.5-m antenna consists of an equatorially mounted parabolic reflector with a Cassegrain feed system and was originally operated as a single antenna telescope (Ref. 4). The 3-m antenna was installed specifically to provide an interferometer in conjunction with the first antenna. It consists of a surplus spun-aluminum reflector which was resurfaced for millimeter work and employs a prime focus feed. An altitude/azimuth mount was obtained by modification of a surplus Nike missile radar tracking mount and includes a transport trailer which allows the antenna to be readily moved. The aperture efficiency of each antenna is approximately 50 percent at 8 mm. The main beam of the interferometer (the product of the individual antenna voltage patterns) has a half-power beamwidth of 8′.

C. The LO System

A centrally located oscillator supplies 12-GHz signals to the receivers through waveguide transmission lines. These signals are tripled in the receivers to provide coherent 36-GHz signals to the mixers. The central oscillator consists of a Gunn diode phase-locked to a crystal standard to provide a 12-GHz output accurate to one part in 10^7. This signal is amplified by a Varian traveling wave tube to a level of approximately 1 W, divided, and transmitted underground through a flexible elliptical waveguide to each antenna site. At each antenna the signal is routed up to the receiver through a thermally insulated waveguide with rotary couplings at the antenna axes. The triplers provide in excess of 10 mW of power at 36 GHz to the mixers. A controlled frequency offset, variable within the range ±1 Hz, is introduced into one of the 12-GHz lines by means of a mechanical phase shifter following the power divider. The rotation of the phase shifter is computer-controlled so that the signal output frequency is precisely maintained at 0.5 Hz.

The relative phase of the 36-GHz signals appearing at the mixers changes due to variations in the effective electrical lengths of the transmission lines following the 12-GHz power division. No effort has been made to control the electrical length difference other than underground burial of the transmission lines and thermal insulation of the antennas where the signals are transported up to the receivers. The relative phase of the LO signals at the mixers is thus subject to slow variations related to ambient conditions. Extensive astronomical observations show that this instrumental phase drift rarely exceeds 20°/h.

D. Receivers

The receivers employ uncooled balanced mixers with Schottky-barrier diodes manufactured by Spacekom, Inc. The system noise temperature of each receiver is approximately 500 K (double sideband) with a rectangular 100-350 MHz IF bandpass flat to within ±0.5 dB. The resulting sensitivity in the measurement of flux density from a point source is better than 0.1 Jy/h. The current mixers were installed in August 1977, prior to which date the receiver characteristics were slightly different (Janssen and Olsen (Ref. 1)). Both antennas receive one linear polarization, with the polarization vector at zero position angle. The feed horn and receiver assembly of the 3-m antenna (which is azimuthally mounted) is rotated to track this polarization.

E. Delay Compensation Network

A gain-balanced network of delay segments is interposed in one IF path to equalize the relative signal delay as a source is tracked across the sky. The delay network consists of 10 cable

pairs and associated high-frequency switches. Each cable pair consists of a fixed length of low-loss coaxial cable and a shorter length of high-loss cable of matched attenuation. One member of each pair is switched into the 3-m antenna signal path as required. The differential delays in each pair form a binary sequence which allows a net delay in the range 0-512 ns to be selected with a resolution of 0.5 ns.

The differential delay of each pair was initially calibrated to an accuracy of ±0.03 ns. These errors were subsequently refined astronomically as described in a following section. With these calibrations we estimate that the net error in a given delay setting is typically about 0.06 ns, with a worst case error of 0.20 ns. These errors lead to signal amplitude losses due to decorrelation of 0.4 and 3 percent, respectively. The finite resolution of the delay network further leads to an average signal loss of less than 1 percent. Residual differences in the attenuations of each cable pair are about 1 percent and are calibrated to reduce the average error from this source to less than 0.5 percent.

F. Gain Calibration

A gas-discharge noise source is weakly coupled to the RF input of each receiver through a directional coupler. When switched on manually each noise source adds approximately 40 K to the total noise power of its associated IF channel. The gains of the IF-mixer networks exhibit slow drifts, of about 1 percent/h, and the noise sources provide a means of monitoring this gain drift. The net gain of the correlated output also depends upon parameters of the correlator itself, but gain variations caused by this component are not significant.

G. Computer Control and Signal Processing

Routine functions of the interferometer are automatically controlled by an Interdata Model 4A computer. These functions include antenna tracking, delay setting, phase shifter rotation, and orientation of the 3-m antenna polarization as well as the processing and analysis of the output signal. The basic cycle of the computer control program is 2 s, during which time the position of the source is recomputed, the interferometer control parameters are monitored and updated, and one complete 0.5-Hz signal cycle (fringe) is obtained. Absolute time-sequencing is provided by a crystal-controlled clock synchronized with the universal time broadcast by the National Bureau of Standards (WWV). The source position along with terms describing its relative motion during the course of the observation are obtained from externally provided ephemerides, and they are entered into the control program at the start of the observation.

The correlator output is integrated and digitized in contiguous 100-ms intervals, and in each 2-s program cycle a complete 20-point sample of the fringe is obtained and stored in the computer. Successive samples are stacked for a preselected number of cycles n, after which the accumulated fringe is analyzed to obtain one complete integration of $2n$-s duration. The fringe amplitude and phase are determined by least squares fit. The residuals of this fit are used to estimate directly the uncertainty of the result, and a record is thereby obtained of the instrumental noise in each individual integration.

III. Performance and Calibration

A. Baseline and Delay Calibration

The extragalactic source 3C273 was observed in May 1974, to obtain an initial determination of the baseline. The two orthogonal components of the baseline which lie in the earth's equatorial plane were subsequently determined by minimizing the diurnal phase drifts in the observation of several sources of known position. Uncertainties of 0.5 wavelengths are estimated for these components. The uncertainties are primarily due to the slow drift in the unregulated instrumental phase. The polar baseline component was determined to ±5 wavelengths by surveying, and this accuracy was verified astronomically by the measurement of delay decorrelation (see below) for sources widely spaced in declination. An effort is currently underway to reduce the uncertainty in this component by the more sensitive technique of astronomical phase measurements, a task which is considerably more difficult at millimeter than at centimeter wavelengths because of the relative scarcity of suitable point sources.

The broad IF bandwidth gives a correspondingly narrow correlation function in the net signal delay at the correlator inputs. Complete signal decorrelation occurs if the absolute delay difference is approximately 1.3 ns. The initial calibration of the delay compensation network was astronomically checked and improved. In principle the shape of the correlation function may be measured, and its center thus determined by adjusting a fixed delay offset in the tracking program while observing a source. In practice we used a technique in which a source was tracked across the sky at the alternate half-power points of the correlation function, where small delay errors produce maximum fluctuations in signal amplitude. Correlation of these fluctuations with the binary delay network setting permits the individual delay element errors to be determined, as well as allowing an upper limit to be placed on the "worst case" setting in which all of the errors are additive. Further, from measurements of several sources one may determine the variation of the correlation function center with declination, from which the polar baseline

component may be estimated. Using this technique we have obtained the above-quoted errors, which are valid for sources within ±30° of the ecliptic.

B. Phase and Amplitude Stability

There are several sources of error in the measurement of the signal phase. System noise causes a random phase error which approaches σ/a rad in the strong signal limit, where a and σ are the amplitude and amplitude uncertainty of a particular measurement. The instrumental phase is generally unknown, and its slow but unpredictable drift contributes to the long-term phase error. Control errors in the phase shifter may result in an instantaneous phase error of up to 2°. Finally, fluctuations in the atmospheric paths of the signals received at each antenna produce a spectrum of phase errors which tends to decorrelate the signal during individual integrations and may scatter phase measurements with a wide range of time scales.

System performance under varying conditions is illustrated by the measurements of Venus shown in Figs. 2 and 3. Near inferior conjunction Venus is one of the strongest millimeter-wavelength sources in the sky, although it is an extended source and is then "resolved" by the interferometer. Generally speaking, a two-element interferometer measures only a single Fourier component of the brightness distribution, the particular component measured depending upon the geometric relationship of the source to the baseline at the instant of observation. The signal produced by an extended source is thus always less than would be obtained if the object were a point source with the same total flux. The ratio, as it depends upon baseline projection, is known as the visibility function (or more correctly, the normalized visibility function). As a rule, the larger the baseline as projected onto the plane of the sky in the direction of the source, the more highly resolved is the source; i.e., the less the "visibility."

The data shown were obtained on two different days near the time of the 1975 inferior conjunction and consist of the signal amplitude and phase obtained in 1-min integrations. Venus rose off the end of the baseline and became progressively more resolved with increasing hour angle in the figures. The solid curves show the theoretical visibility functions and phases computed for a uniformly bright disk at the locations and with the semidiameters given for Venus in the American Ephemeris and Nautical Almanac on the dates of observation.

The amplitudes have been corrected for atmospheric attenuation, which has been taken from a theoretical model to be a constant 3 percent at the zenith, and to scale as the secant of the zenith angle. About two-thirds of this attenuation is due to atmospheric oxygen and is effectively constant, with water vapor accounting for the remainder. The variability of water vapor under typical observing conditions is expected to lead tc errors less than 1.5 percent in amplitude measurement. The phase data have been corrected to remove a small sinusoidal phase drift of 24-h period to allow for residual baseline errors and the diurnal component of the instrumental phase drift.

The amplitude scale of the data shown in Fig. 2 has been adjusted to give a least-squares fit to the calculated visibility function. These data were obtained under normal observing conditions when the weather was clear and stable. The amplitude scatter is small and uniform as the signal amplitude varies and is consistent with that expected due to receiver noise. Where the signal is small the phase scatter is generally consistent with the noise-to-signal ratio σ/a, with the phase becoming random at about the time the signal disappears. For signals of relative amplitude (visibility) greater than about 0.15, however, the rms phase scatter approaches a lower limit of about 3°, which reflects the combined effects of instrumental and atmospherically induced phase noise. This demonstrates that the instrumental performance is within expected bounds and that the atmosphere's influence under "good" weather conditions is minimal.

Because the real part of the index of refraction of air is very nearly constant with frequency throughout the microwave region, the atmospherically induced phase fluctuations for a given baseline will increase linearly with the observing frequency. One may therefore anticipate that atmospheric conditions are of greater concern at millimeter wavelengths than in the centimeter range. The data shown in Fig. 3 were obtained under poor observing conditions, with thick cumulus clouds over the interferometer. The observing parameters were substantially the same in both observations, and the curve shows the expected amplitude of the signal based on the calibration of the data of Fig. 2. The amplitude scatter is seen to depend on amplitude and indicates signal losses approaching 50 percent for individual 1-min integrations. We attribute this loss to large short-term phase fluctuations due to atmospheric inhomogeneities which decorrelate the signal on time scales less than 1 min. The phase scatter among the 1-min integrations, even where the signal is large, shows fluctuations up to 60°, and indicates that substantial atmospheric effects are present on time scales on the order of 1 min. These data illustrate the particular importance of weather conditions on interferometric observations at millimeter wavelengths.

C. Future Modifications

The interferometer is currently undergoing modification to accommodate a program of solar flare observations. The principal change will be the conversion of the receiver polarization from a single linear mode to dual circular modes in which either left- or right-circular polarizations may be selected. Rapid switching will permit alternate polarizations to be received in contiguous integrations as short as 2 s.

Acknowledgments

We gratefully acknowledge the participation of Glenn Berge in the initial planning stages of the interferometer and the technical assistance of Richard Wetzel in its construction. The Table Mountain interferometer was constructed and is operated under Contract NAS 7-100, sponsored by the National Aeronautics and Space Administration.

References

1. M. A. Janssen and E. T. Olsen, "A measurement of the brightness temperature of Saturn's rings at 8-mm wavelength," *Icarus*, vol. 33, pp. 263-278, Feb. 1978.
2. M. A. Janssen, E. T. Olsen, and K. R. Lang, "Interferometric observations of the quiet Sun at 8-mm wavelength," *Astrophys. J.*, vol. 228, pp. 616-628, March 1979.
3. W. N. Christiansen and J. N. Hogbom, *Radiotelescopes*. Cambridge: Cambridge University Press, 1969.
4. J. R. Cogdell, J. J. G. McCue, P. D. Kalachev, A. E. Salomonovich, I. G. Moiseev, J. J. Stacey, E. E. Epstein, E. E. Altshuler, G. Feix, J. W. B. Day, H. Hvatum, W. J. Welch, and F. T. Barath, "High resolution millimeter reflector antennas," *IEEE Trans. Antennas and Propagat.*, vol. AP-18, pp. 515-529, July 1970.

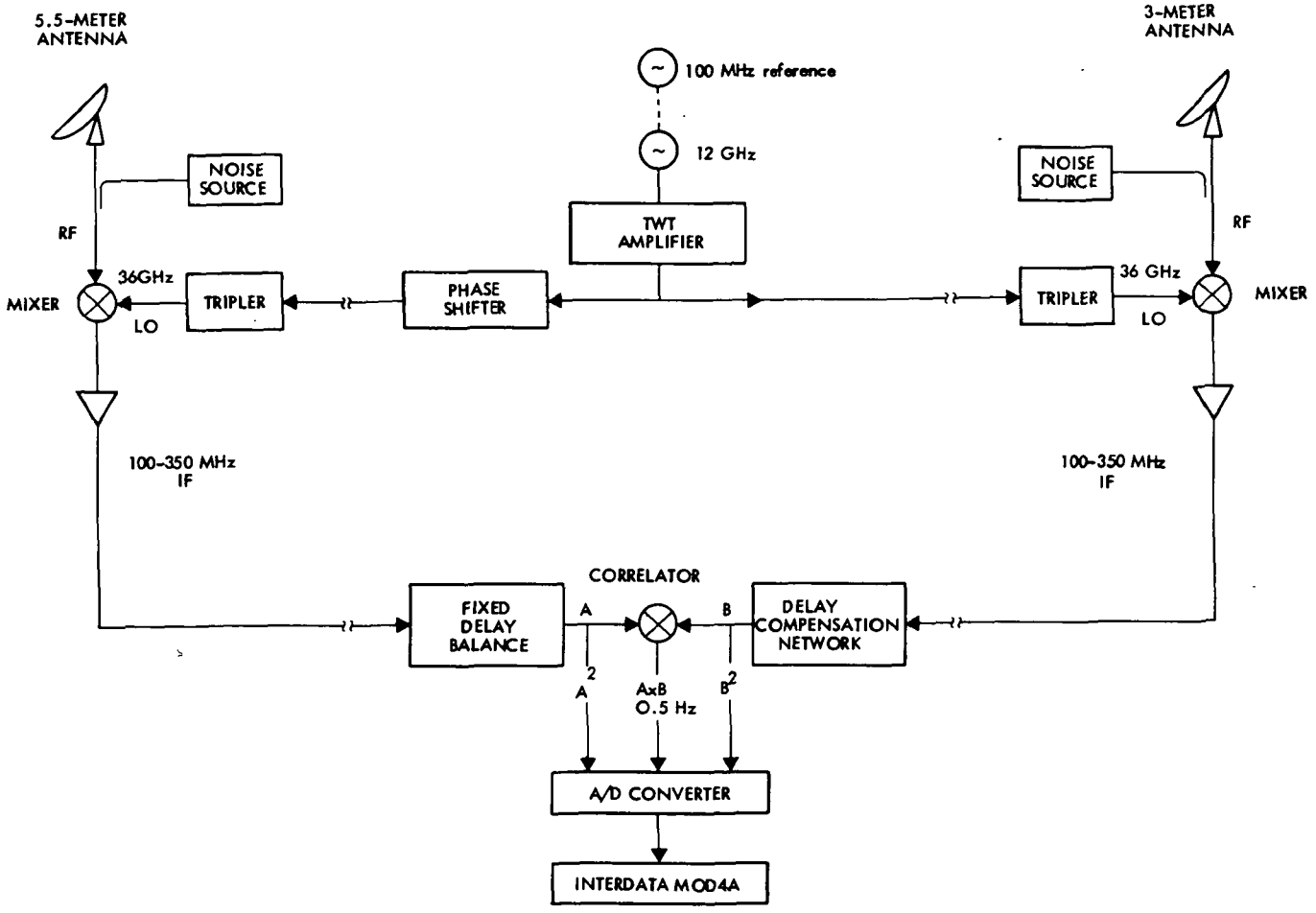

Fig. 1. Schematic diagram of the Table Mountain 8-mm interferometer system

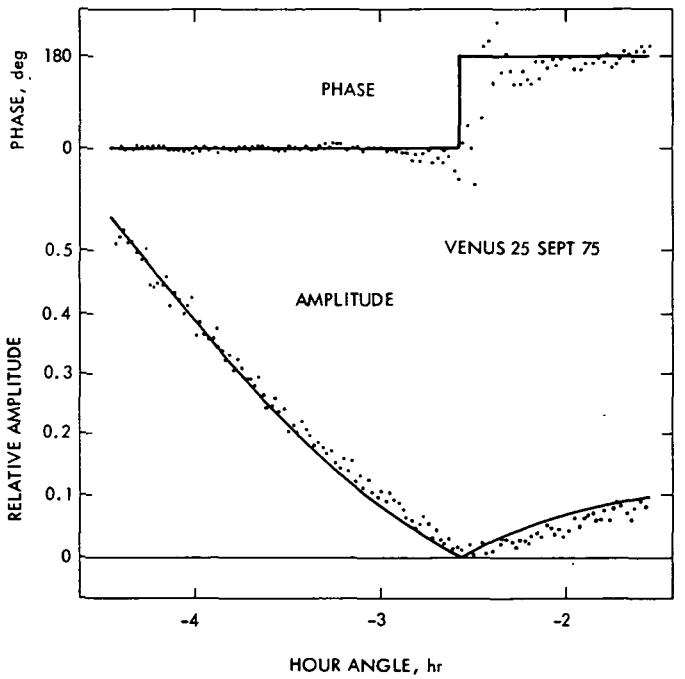

Fig. 2. Data from Venus observations September 25, 1975. Points show phase and amplitude obtained in contiguous 1-min integrations. Venus becomes progressively resolved during the course of the observations, with an amplitude null and 180° phase change near −2.5 h. Curves indicate the behavior expected according to a simple theoretical model; the systematic departure of the data from the amplitude curve is consistent with the expected amount of limb darkening on Venus

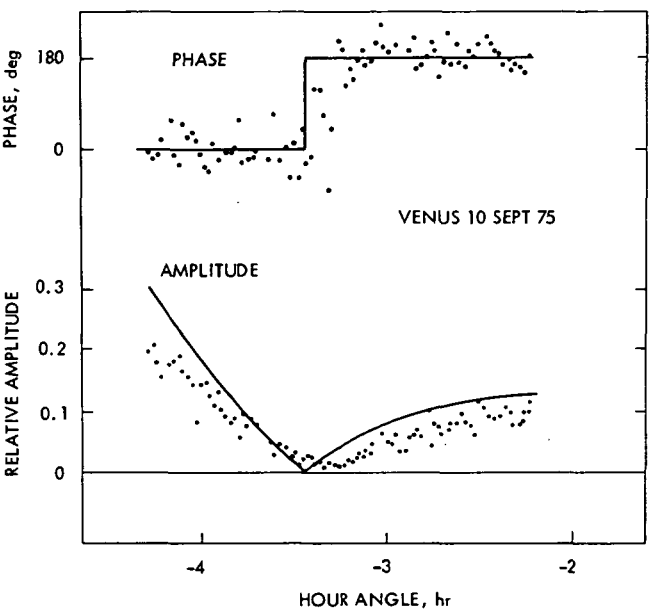

Fig. 3. Data from Venus observations September 10, 1975 which show the extreme effects produced by the atmosphere under poor weather conditions. The observing parameters were substantially the same as for the data of Fig. 2. The data show loss of signal amplitude as well as excessive scatter